Integrating polarization conversion and nearly perfect absorption with multifunctional metasurfaces

Hua Cheng, Xiaoyun Wei, Ping Yu, Zhancheng Li, Zhe Liu, Junjie Li, Shuqi Chen, and Jianguo Tian

Citation: Appl. Phys. Lett. **110**, 171903 (2017); doi: 10.1063/1.4982240
View online: http://dx.doi.org/10.1063/1.4982240
View Table of Contents: http://aip.scitation.org/toc/apl/110/17
Published by the American Institute of Physics

Integrating polarization conversion and nearly perfect absorption with multifunctional metasurfaces

Hua Cheng,[1] Xiaoyun Wei,[1] Ping Yu,[1] Zhancheng Li,[1] Zhe Liu,[2] Junjie Li,[2] Shuqi Chen,[1,a)] and Jianguo Tian[1]
[1]*The Key Laboratory of Weak Light Nonlinear Photonics, Ministry of Education, School of Physics and TEDA Institute of Applied Physics, Nankai University, Tianjin 300071, China*
[2]*Beijing National Laboratory for Condensed Matter Physics, Institute of Physics, Chinese Academy of Sciences, P.O. Box 603, Beijing 100190, China*

(Received 14 February 2017; accepted 13 April 2017; published online 27 April 2017)

Manipulating electromagnetic waves with artificial nanostructures has garnered great interest for their properties and potential applications. However, existing devices performing various desired operations at different wavelengths usually require cascading with different geometry patterns, which does not offer satisfactory simplicity. Here, we theoretically and experimentally demonstrate that an ultrathin, multifunctional metasurface, consisting of an array of nanorods, can perform various functions at different wavelengths. Simulated and experimental results indicate that nearly perfect absorption, linear-to-circular conversion, and linear cross-polarization conversion can be integrated into one multifunctional metasurface. Furthermore, the multifunctional metasurface can maintain very high performance across a large range of incident angles. The proposed configuration is extremely compact and easy to fabricate; these qualities should support the development of practical applications. *Published by AIP Publishing*. [http://dx.doi.org/10.1063/1.4982240]

The development of metamaterials has led to a diversity of exciting and profound effects that depend upon modulated electromagnetic waves generated by manipulating the reflection mode through adjustments to the interaction between the incident wave and the components of the engineered configuration.[1,2] Extensive pioneering research has exhibited significant accomplishments over the past few years and demonstrated that the precise arrangement of elements can be shaped to exhibit desired changes in the amplitude and phase of the scattered light response.[3–5] Among engineered nanostructures, metasurfaces showing ultrathin planar configurations that can alter the phase of the incident light abruptly at the interface attract growing attention because of their remarkable versatility and ease of fabrication in comparison to their bulk counterparts.[6–8]

The unique optical properties of metasurfaces support the generation of many extraordinary physical phenomena, such as polarization conversion,[9–12] anomalous reflection,[13] nearly perfect absorption,[14,15] metasurface holograms,[16] and planar perfect lenses.[17] In these cases, two lines of research investigations of polarization conversion and developments of metasurface-based optical resonators have progressed significantly. Substantial studies have indicated that many exceptional manipulations of the polarization state or intensity of light can manifest high efficiency,[18] wide operating-wave bands,[19] wide incident angles and polarization insensitivity,[20] and dynamically reconfigurable optical responses.[21,22]

Despite these works to utilize metasurfaces to realize exotic performance, only an expected operating function can be produced at a specific wave band. Chen *et al*. have realized multifunctional metasurfaces' lens or hologram, which also demonstrated the importance and interest for multifunctional metasurfaces.[23,24] Nevertheless, practical applications have demonstrated, through miniaturization and simplification, the integration of a single nanostructure with a multifunction metasurface. A survey of research shows that several designs have proposed full-wave operational devices performing various functions at different frequencies. However, in these designs, geometries with different dimensions or engineered patterns must be arranged into one supercell to support independently operating functions that can, in turn, be merged into a multifunctional device. Such devices are relatively difficult to fabricate and impractical for use in working systems.[25]

In this letter, we theoretically and experimentally demonstrate that an ultrathin, multifunctional metasurface consisting of a nanorod array can achieve different functions at different wavelengths. We demonstrate that nearly perfect absorption and either linear-to-circular conversion or linear cross-polarization conversion can be integrated into one double-functional metasurface and operated at different frequencies. Subsequently, we prove that linear cross-polarization conversion, linear-to-circular conversion, and nearly perfect absorption can be realized simultaneously by optimizing further the geometric parameters to form multifunctional metasurfaces. We also study the angular dispersions of the reflective amplitude and phase difference and prove that the proposed multifunctional metasurface can work across a wide range of incident angles. Based on the configuration of the metal-dielectric-metal (MDM) device, various reflective manipulations can be merged into one single metasurface. This result serves as a further step in developing multifunctional metasurfaces for use in electromagnetic devices.

The construction of a device that not only can act as a perfect absorber but also can convert the polarization state of incident light depends upon a design that prohibits in-system

a)Author to whom correspondence should be addressed. Electronic mail: schen@nankai.edu.cn

transmission and provides simultaneous tuning of the phase and amplitude of reflected light at relevant wavelengths. An MDM configuration can meet these requirements. A continuous metal layer can prevent the transmission of any incident light through the system. The localized plasmon resonance and the magnetic resonance induced by the incident electromagnetic wave in the metal layers can block and counteract the original energy, yielding near-zero reflection around the resonant frequency.

The top metal layer should be a homogeneous anisotropic metasurface composed of metallic nanoresonator arrays to support adjusting the phase of reflected light. We employed gold nanorods as individual inclusions because (1) the dimensions of this simple geometry optimize conveniently to provide the desired phase change and (2) precise nanoscale device fabrication is much easier. A nanorod can be treated as two orthogonal resonators exhibiting no interaction along the long and short nanorod axes, respectively. The resonance frequencies ω_{px} and ω_{py} are determined by the nanorod dimensions. Then, the polarizabilities $\alpha_{x(y)}$ are expressed by

$$\alpha_{x(y)}(\omega) = \frac{A\omega_{px(y)}^2}{\omega_{px(y)}^2 - \omega^2 - i\Gamma\omega}, \tag{1}$$

where A represents the intensity and Γ denotes the damping coefficient.

Intermediate incident light with polarization along the orientation between the x and y directions can exhibit excitation of both dipoles. The amplitudes of the polarizabilities are almost equal in the wavelength range in which the desired functionality works. Then, the phase difference of the two polarizabilities for minimal offset $\omega = \frac{\omega_{px}+\omega_{py}}{2} \gg \frac{\omega_{px}-\omega_{py}}{2}$ can be expressed as a function of $\omega_{px} - \omega_{py}$,[26]

$$\Delta\Phi\left(\frac{\omega_{px}+\omega_{py}}{2}\right) = (\Phi_1 - \Phi_2)_{\omega=\frac{\omega_{px}+\omega_{py}}{2}} = \pi - \arctan\left(\frac{\Gamma}{\omega_{px}-\omega_{py}}\right). \tag{2}$$

By adjusting the magnitude of the width w and aspect ratio w/l of an isolated nanorod to change the values of ω_{px} and ω_{py}, we can design waveplates exhibiting arbitrary measures of retardation. Meanwhile, the metal layer plays a critical role in increasing the reflection coefficient and polarization conversion ratio through the superposition of the reflected fields credited to the modified Fabry-Pérot etalon formed with the top gold nanorod arrays. The dielectric spacer, owing to the addition of optical distance, can increase the design degree to expand the range of phase difference. The interaction of all elements easily yields polarization conversion with high reflection.

Here, we propose a series of multifunctional metasurfaces and investigate their reflection properties. Figure 1(a) shows the schematic of the proposed multifunctional metasurface, which comprises a top homogeneous anisotropic metasurface, a silicon dioxide layer separated from the metasurface by a subwavelength air spacer, and a bottom continuous gold layer. The unit cell is illustrated in Fig. 1(b). The incident linearly polarized plane wave exhibits polarization relative to the x axis in the x–y plane. The reflected light can be realized either as

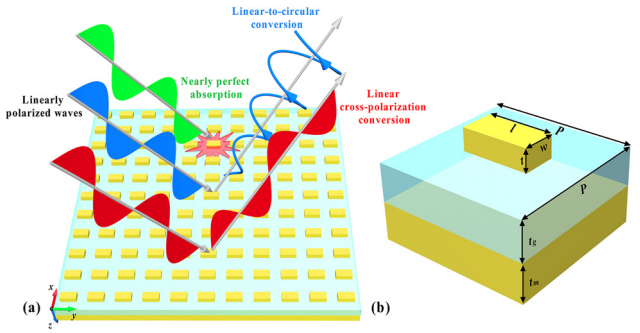

FIG. 1. Schematic representations of the proposed multifunctional metasurface. (a) A depiction of simultaneously realized linear cross-polarization conversion, linear-to-circular conversion, and nearly perfect absorption. (b) The unit cell of the proposed multifunctional metasurface.

nearly perfect absorbed or as converted either to a linearly cross-polarized wave or to circularly polarized light. The form of polarization can be selected arbitrary by appropriately designing the nanostructure. The theoretical simulations were performed using a commercial software package, COMSOL Multiphysics (COMSOL Inc., Burlington, MA), based on the finite element method. The Drude model defines the material properties of gold: a relative permittivity at infinite frequency $\varepsilon_\infty = 9.0$, plasma frequency $\omega_p = 1.3166 \times 10^{16}\text{s}^{-1}$, and damping constant $\gamma = 1.3464 \times 10^{14}\,\text{s}^{-1}$.[27] The refractive index of the glass substrate is taken to be 1.47. In these theoretical simulations, the unit cell has periodic boundary conditions in the x and y planes and waveguide ports boundary conditions on the other boundaries.

We first consider the design of a double-functional metasurface. Figure 2(a) shows the simulated reflection coefficients and phase difference between x- and y-polarizations of the reflected light illuminated by a linearly polarized incident light with polarization direction 45° relative to the x axis. The results show that the amplitudes of the x and y components are high and remain almost invariable in the range of 1300 nm to 1400 nm. The phase difference can reach 90° at a wavelength of 1352 nm, which ensures that the reflected light is perfectly circular-polarized radiation. To experimentally verify the theoretical results, we fabricated the proposed double-multifunctional metasurface using electron beam lithography. Figure 2(b) shows the top view of the scanning electron microscopy (SEM) image of the fabricated sample. We illustrate the polarization conversion ability of our design by giving the polarization states of the reflected light at 1352 nm in a simulation and 1295 nm in an experiment, as shown in Figs. 2(c) and 2(d), respectively. Both the theoretical and experimental results suggest that the reflected light can be converted into circularly polarized light (red curve) incident by the linearly incident light polarized along angles of 43° and 32° (blue curves). The simulated and experimental conversion efficiencies are 42.7% and 22.6%, respectively. In addition, the simulated and experimental absorption spectra of the designed double-functional metasurface are given in Figs. 2(e) and 2(f). An apparent nearly perfect absorption at 775 nm can be obtained. The absorption effect is due to the excitation of localized electric dipole resonances in the metallic nanobars. In addition, surface currents in the top metallic nanobars and the ground metallic

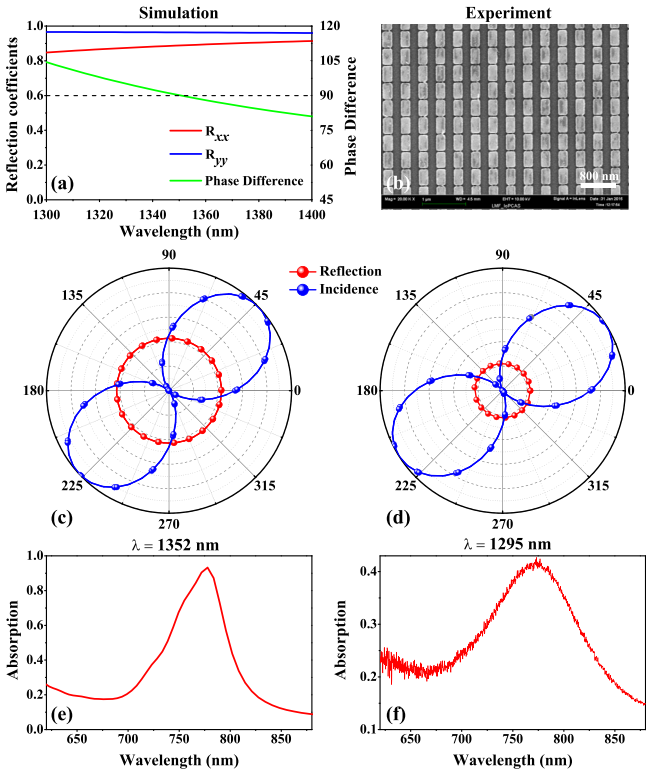

FIG. 2. Comparison of simulation and experimental metasurface performance of linear-to-circular conversion and related absorption spectra. (a) Simulated reflection coefficients and phase difference between the *x*- and *y*-polarizations of reflection light spectra illuminated by the linearly polarized incident light with a polarization direction of 45° relative to the *x* axis. The length *l*, width *w*, and thickness *t* of the nanorod are 350 nm, 180 nm, and 55 nm, respectively. The lattice constant *P* in both the *x* and *y* directions is 400 nm. The thicknesses t_g and t_m of the SiO_2 spacer and bottom continuous gold layer are 30 nm and 100 nm, respectively. (b) A SEM image showing the top view of the fabricated double-functional metasurface. (c) Simulated and (d) experimental linear-to-circular conversion at 1352 nm and 1259 nm, respectively. (e) Simulated and (f) experimental absorption spectra for the proposed double-functional metasurface.

plane are opposite to each other. The magnetic field accumulates in the dielectric spacer between them. Magnetic dipole resonances also contribute to the absorption effect. The experimental result shows reasonable agreement with the simulated result, partly because of the inclined incidence in the experiment and inaccuracies occurring during fabrication. The absorption performance of the proposed devices was simulated with normal incidence with the polarization direction along the long axis of the nanorod. For our experimental measurement, a Bruker VERTEX 70 spectrometer was used to focus the incident wave on the sample with a near-infrared microscope objective. The measurement result is an average value for wide incident angles. Thus, the main reason for the discrepancy between the simulated and measured absorption spectrum is about different incident angles. Furthermore, for the measurement, the polarization angle may not be strictly along the long axis of the nanorods, which also affects the absorption strength. Consequently, our designed double-functional metasurface can provide simultaneous integration of the functionality of a nearly perfect absorber in the visible spectrum and linear-to-circular conversion in the near-infrared range.

The double-functional metasurface can incorporate geometric parameters designed to provide the simultaneous functions of linear-to-linear conversion with cross polarization and linear-to-circular conversion at different frequencies. Figure 3(a) depicts the simulated reflection coefficients and phase difference between *x*- and *y*-polarizations of the reflected light spectra illuminated by linearly polarized incident light with a polarization direction of 45° relative to the *x* axis. The phase difference can be controlled easily to reach 180° at 1131 nm and 90° at 1368 nm, respectively. The corresponding amplitude can maintain a high value simultaneously. The SEM image of the fabricated sample, viewed from the top, is also shown in Fig. 3(b). Figures 3(c) and 3(d) show the simulated and experimental linear cross-polarization conversions, which can convert linearly polarized light to its cross polarization in the reflection mode. The experimental results show good agreement with the simulated results except that the working wavelength of 1228 nm displays a redshift. Meanwhile, we also prove that the linearly polarized light can be converted easily into circularly polarized light by using the same geometric configuration. The simulated and experimental results are shown in Figs. 3(e) and 3(f), respectively. We see there that the incident

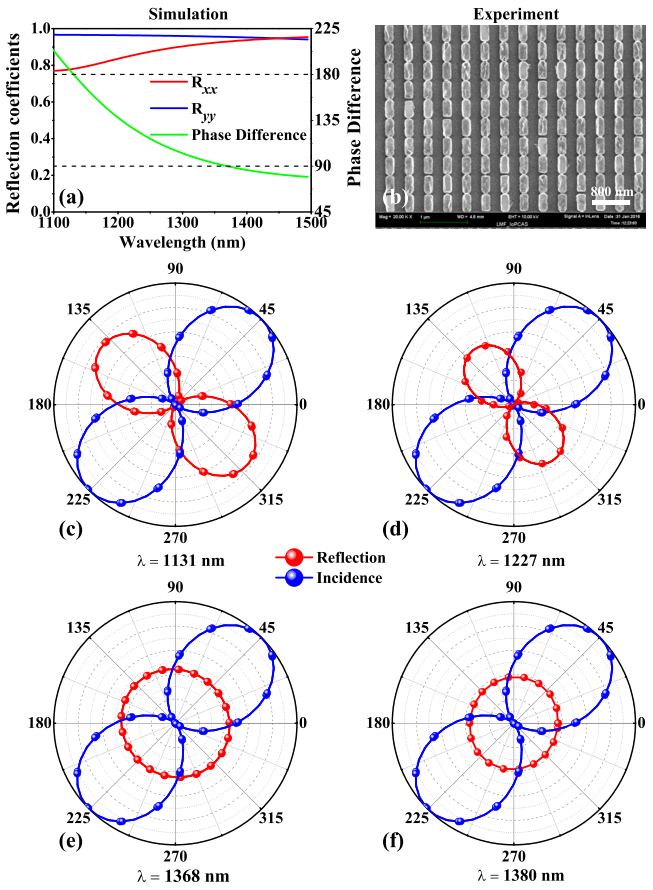

FIG. 3. Comparison of simulation and experimental metasurface performance of linear cross-polarization and linear-to-circular conversions. (a) Simulated reflection coefficient and phase difference between *x*- and *y*-polarizations of reflection light spectra illuminated by the linearly polarized incident light with a polarization direction of 45° relative to the *x* axis. The length *l*, width *w*, and thickness *t* of the nanorod are 350 nm, 175 nm, and 40 nm, respectively. The thickness t_g of the SiO_2 spacer is 50 nm. The period of the nanorod is 400 nm. (b) A SEM image showing the top view of the fabricated double-functional metasurface. (c) Simulated and (d) experimental linear cross-polarization conversion at 1131 nm and 1227 nm, respectively. (e) Simulated and (f) experimental linear-to-circular conversion at 1368 nm and 1380 nm.

linearly polarized light can be converted effectively into circularly polarized light, with conversion efficiencies of 45.2% and 38.0% at 1368 nm and 1380 nm, respectively. It should be noted that there exists coupling between the gold nanorods, especially along the direction of the long axis of the nanorods. However, the coupling between the nanorods has little influence on the amplitude and phase difference because the wavelengths of polarization conversions are out of the resonance.

The multifunctional metasurface, which can achieve the simultaneous functions of linear cross-polarization conversion, linear-to-circular conversion, and nearly perfect absorption, also can be obtained by further optimizing the geometric parameters, as shown in Fig. 4. The reflection coefficients and the phase difference between the *x*- and *y*-polarizations are shown in Fig. 4(a). The phase difference can achieve angles of 90° and 180° at 1267 nm and 1151 nm with high reflection coefficients, respectively. Figure 4(b) shows the associated SEM image with optimized geometric parameters. Figures 4(c) and 4(d) show the simulated and experimental linear cross-polarization conversions, which are in reasonable agreement with each other. Although the experimental result is tripled at the low experimental efficiency, we demonstrate that the reflected light is normal linear light polarized at an angle of 113° with incident light polarized at an angle of 23°. This result confirms that the proposed multifunctional metasurface can perfectly realize cross-polarization conversion. Figures 4(e) and 4(f) theoretically and experimentally demonstrate that linearly polarized light also can be converted into circularly polarized light by using the same geometrical configuration at a different wavelength. The polarizations of the incident light align with angles of 36° at 1267 nm and 23° at 1394 nm for the simulated and experimental results, respectively. The experimental result is also multiplied by three, as indicated in Fig. 4(f), to confirm the converted circularly polarized light. The simulated and experimental absorption spectra of the multifunctional metasurface also are shown in Figs. 4(g) and 4(h), respectively. The simulated nearly perfect absorption at 770 nm can be achieved. The absorption peak for the experimental result is relatively low compared to the absorption peak for the simulated result because of the inclined incidence in the experiment and the inaccuracies of fabrication.

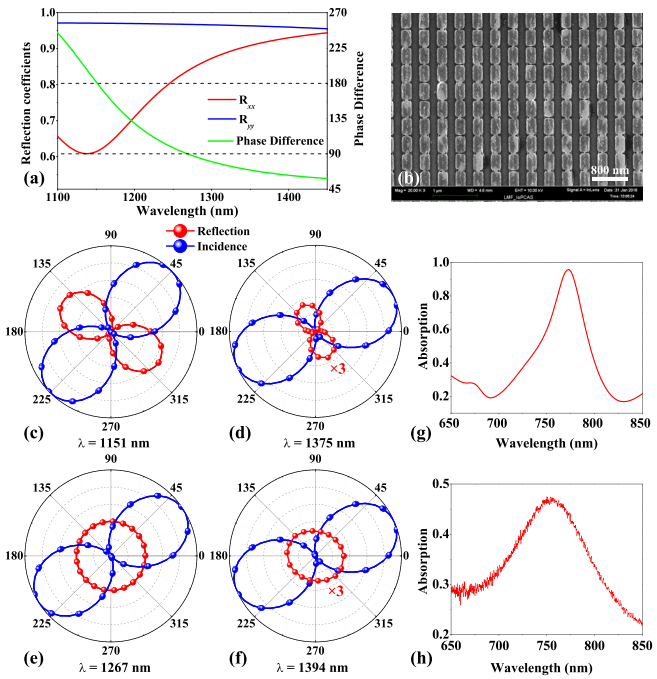

FIG. 4. Comparison of simulation and experimental metasurface performance of linear cross-polarization, linear-to-circular conversions, and related absorption spectra. (a) Simulated reflection coefficient and phase difference between *x*- and *y*-polarizations of the reflection light spectra illuminated by the linear-polarized incident light with a polarization direction of 45° relative to the *x* axis. The length *l*, width *w*, and thickness *t* of the nanorod are 350 nm, 175 nm, and 40 nm, respectively. The thickness t_g of the SiO_2 spacer is 30 nm. The period of the nanorod is 400 nm.(b) A SEM image showing the top view of the fabricated multifunctional metasurface. (c) Simulated and (d) experimental linear cross-polarization conversion at 1151 nm and 1375 nm, respectively. (e) Simulated and (f) experimental linear-to-circular conversion at 1267 nm and 1394 nm, respectively. (g) Simulated and (h) experimental absorption spectra for the proposed multifunctional metasurface.

The angle insensitive performance is important in practical applications. In some cases, most of the obtainable light, needed for operations, may contain a wide range of incident angles. We plotted the angular dispersion of the reflective amplitude to investigate both the angle dependence of the proposed multifunctional metasurface, as shown in Figs. 5(a) and 5(c), and the phase difference between the *x*- and *y*-polarizations at 1150 nm, as shown in Figs. 5(b) and 5(d). In the plots in Fig. 5, the alignment was oblique in the *x*–*z* and *y*–*z* planes. The angle of incidence is defined as the angle between the wavevector and the *z* axis of the corresponding coordinate. For oblique angles in the *x*–*z* plane, the reflective amplitude and phase difference show slight variations across a large range of incident angles. When the angles are oblique in the *y*–*z* plane, the reflective amplitude and phase difference will gradually decrease with increasing incident angles. In this case, the components of the electromagnetic wave used to drive electric dipoles in the metallic nanorod decrease.

For our designed nanobar metasurface, only one functionality dominates at one wavelength (i.e., perfect absorption,

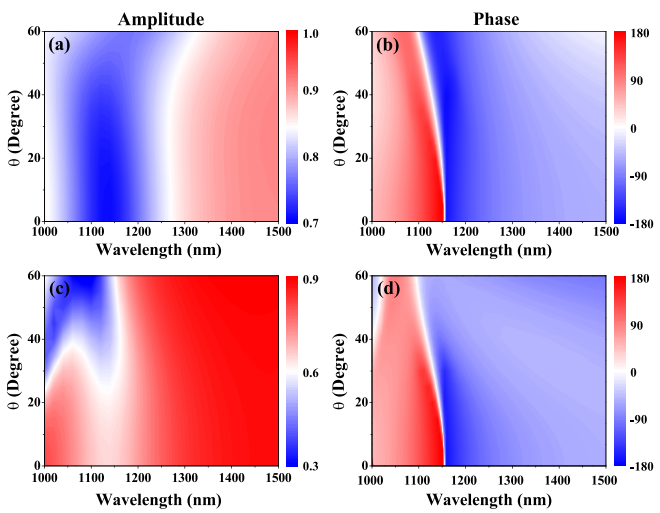

FIG. 5. Simulated reflective amplitude and phase differences. (a) and (c) The angular dispersion of the reflective amplitudes. (b) and (d) The distribution of phase differences. The simulations modeled *x*- and *y*-polarizations as functions of wavelength and angle of incidence under 1150 nm incident light oblique in the *x*-*z* and *y*-*z* planes.

linear-to-circular conversion, or linear cross-polarization conversion). Perfect absorption will absorb the light along y polarization. However, linear-to-circular conversion or linear cross-polarization conversion requires nonzero y component of light. Thus, perfect absorption cannot be achieved simultaneously with linear-to-circular conversion or linear cross-polarization conversion. Furthermore, for our designed nanobar structure, $\Delta\Phi = \Phi_{xx} - \Phi_{yy}$ is just related to the structure parameter and wavelength. Fixed structure parameter and wavelength will lead to a fixed $\Delta\Phi$, which should be $\pi/2$ for linear-to-circular conversion and π for linear cross-polarization conversion. Thus, the linear-to-circular conversion and the linear cross-polarization conversion cannot be achieved simultaneously.

In summary, we have theoretically and experimentally demonstrated that multi-functional devices with high efficiency and scalability can be fabricated using a simple configuration based on MDM. Depending on the frequency-selective reflective radiation of nanorods, such arrays perform desired effects at particular frequencies that can be adjusted carefully without recourse to complicated geometric designs and arrangements. These qualities made fabrication extremely convenient. We verified the results of our design simulation by carrying out experimental measurements, which showed a good match with the predictions obtained from the theoretical model. Furthermore, in addition to supporting the integration of several functions, this design also features thickness far less than the operated wavelength. Thus, our design shows prospects for applications in micro-optics. With its excellent performance and compactness, our design can add value to many practical applications, such as simultaneous sensing and polarization. This configuration capacity for supporting elaborate patterns and dimensional designs can enable the creation of structures that integrate additional useful functions in the full-wave band and increase miniaturization and versatility.

This work was supported by the National Key Research and Development Program of China (2016YFA0301102), the Natural Science Foundation of China (11574163 and 61378006), the Program for New Century Excellent Talents in University (NCET-13–0294), and 111 Project (B07013). We also acknowledge the support from the Collaborative Innovation Center of Extreme Optics, Shanxi University, Taiyuan, Shanxi 030006, China.

[1]D. R. Smith, W. J. Padilla, D. C. Vier, S. C. Nemat-Nasser, and S. Schultz, "Composite medium with simultaneously negative permeability and permittivity," Phys. Rev. Lett. **84**, 4184–4187 (2000).
[2]R. A. Shelby, D. R. Smith, and S. Schultz, "Experimental verification of a negative index of refraction," Science **292**, 77–79 (2001).
[3]J. B. Pendry, D. Schurig, and D. R. Smith, "Controlling electromagnetic fields," Science **312**, 1780–1782 (2006).
[4]N. I. Landy, S. Sajuyigbe, J. J. Mock, D. R. Smith, and W. J. Padilla, "Perfect metamaterial absorber," Phys. Rev. Lett. **100**, 207402 (2008).
[5]G. Dolling, C. Enkrich, M. Wegener, C. M. Soukoulis, and S. Linden, "Simultaneous negative phase and group velocity of light in a metamaterial," Science **312**, 892–894 (2006).
[6]N. Yu, P. Genevet, M. A. Kats, F. Aieta, J.-P. Tetienne, F. Capasso, and Z. Gaburro, "Light propagation with phase discontinuities: Generalized laws of reflection and refraction," Science **334**, 333–337 (2011).
[7]N. Yu, F. Aieta, P. Genevet, M. A. Kats, Z. Gaburro, and F. Capasso, "A broadband, background-free quarter-wave plate based on Plasmonic metasurfaces," Nano Lett. **12**, 6328–6333 (2012).
[8]A. V. Kildishev, A. Boltasseva, and V. M. Shalaev, "Planar photonics with metasurfaces," Science **339**, 1232009 (2013).
[9]A. Roberts and L. Lin, "Plasmonic quarter-wave plate," Opt. Lett. **37**, 1820–1822 (2012).
[10]A. Pors, M. G. Nielsen, G. Della Valle, M. Willatzen, O. Albrektsen, and S. I. Bozhevolnyi, "Plasmonic metamaterial wave retarders in reflection by orthogonally oriented detuned electrical dipoles," Opt. Lett. **36**, 1626–1628 (2011).
[11]Z. Liu, Z. Li, J. Li, H. Cheng, P. Yu, W. Liu, C. Tang, C. Gu, J. Li, S. Chen, and J. Tian, "High performance broadband circularly polarized beam deflector by mirror effect of multi-nanorod metasurfaces," Adv. Funct. Mater. **25**, 5428–5434 (2015).
[12]Z. Li, W. Liu, H. Cheng, S. Chen, and J. Tian, "Realizing broadband and invertible linear-to-circular polarization converter with ultrathin single-layer metasurface," Sci. Rep. **5**, 18106 (2015).
[13]S. Sun, K.-Y. Yang, C.-M. Wang, T.-K. Juan, W. T. Chen, C. Y. Liao, Q. He, S. Xiao, W.-T. Kung, G.-Y. Guo, L. Zhou, and D. P. Tsai, "High-efficiency broadband anomalous reflection by gradient meta-surfaces," Nano Lett. **12**, 6223–6229 (2012).
[14]N. Liu, M. Mesch, T. Weiss, M. Hentschel, and H. Giessen, "Infrared perfect absorber and its application as plasmonic sensor," Nano Lett. **10**, 2342–2348 (2010).
[15]B. Zhang, Y. Zhao, Q. Hao, B. Kiraly, I.-C. Khoo, S. Chen, and T. J. Huang, "Polarization-independent dual-band infrared perfect absorber based on a metal-dielectric-metal elliptical nanodisk array," Opt. Express **19**, 15221–15228 (2011).
[16]G. Zheng, H. Mhlenbernd, M. Kenney, G. Li, T. Zentgraf, and S. Zhang, "Metasurface holograms reaching 80% efficiency," Nat. Nanotechnol. **10**, 308–312 (2015).
[17]Q. Yang, J. Gu, D. Wang, X. Zhang, Z. Tian, C. Ouyang, R. Singh, J. Han, and W. Zhang, "Efficient flat metasurface lens for terahertz imaging," Opt. Express **22**, 25931–25939 (2014).
[18]R. Li, Z. Guo, W. Wang, J. Zhang, A. Zhang, J. Liu, S. Qu, and J. Gao, "High-efficiency cross polarization converters by plasmonic metasurface," Plasmonics **10**, 1167–1172 (2015).
[19]F. Ding, Z. Wang, S. He, V. M. Shalaev, and A. V. Kildishev, "Broadband high-efficiency half-wave plate: A supercell-based plasmonic metasurface approach," ACS Nano. **9**, 4111–4119 (2015).
[20]S. Chen, H. Cheng, H. Yang, J. Li, X. Duan, C. Gu, and J. Tian, "Polarization insensitive and omnidirectional broadband near perfect planar metamaterial absorber in the near infrared regime," Appl. Phys. Lett. **99**, 253104 (2011).
[21]J. Li, P. Yu, H. Cheng, W. Liu, Z. Li, B. Xie, S. Chen, and J. Tian, "Optical polarization encoding using graphene-loaded plasmonic metasurfaces," Adv. Opt. Mater. **4**, 91–98 (2016).
[22]D. Wen, F. Yue, M. Ardron, and X. Chen, "Multifunctional metasurface lens for imaging and fourier transform," Sci. Rep. **6**, 27628 (2016).
[23]D. Wen, S. Chen, F. Yue, K. Chan, M. Chen, M. Ardron, K. Li, P. Wong, K. Cheah, E. Pun, G. Li, S. Zhang, and X. Chen, "Metasurface device with Helicity-dependent functionality," Adv. Opt. Mater. **4**, 321–327 (2016).
[24]H. Cheng, S. Chen, P. Yu, X. Duan, B. Xie, and J. Tian, "Dynamically tunable plasmonically induced transparency in periodically patterned graphene nanostrips," Appl. Phys. Lett. **103**, 203112 (2013).
[25]V. S. Asadchy, Y. Radi, J. Vehmas, and S. A. Tretyakov, "Functional metamirrors using bianisotropic elements," Phys. Rev. Lett. **114**, 095503 (2015).
[26]A. B. Evlyukhin, S. I. Bozhevolnyi, A. Pors, M. G. Nielsen, I. P. Radko, M. Willatzen, and O. Albrektsen, "Detuned electrical dipoles for plasmonic sensing," Nano Lett. **10**, 4571–4577 (2010).
[27]*Handbook of Optical Constants of Solids II*, edited by E. D. Palik (San Diego, Academic Press, 1998).